

High Resolution Capabilities of MIMO Radar

Nikolaus H. Lehmann*, Alexander M. Haimovich*, Rick S. Blum[†], Len Cimini[‡]

* New Jersey Institute of Technology, University Heights, Newark, NJ 07102, email: lehmann, haimovich@njit.edu

[†] Lehigh University, 19 Memorial Drive West, Bethlehem, PA 18015, email: rblum@eecs.lehigh.edu.

[‡] University of Delaware, 208 Evans Hall, Newark, DE 19716, email: cimini@ece.udel.edu.

Abstract—Multiple-input multiple-output (MIMO) radar is a multistatic architecture composed of multiple transmitters and receivers, which seeks to exploit the spatial diversity of radar backscatter. In conjunction with centralized processing, MIMO radar has the potential to significantly improve radar functions such as detection and parameter estimation. MIMO radar is distinct from other types of array radars such as phased array or STAP, which process the signals of closely spaced elements and, hence, cannot capitalize on the spatial characteristics of targets. In this work, we explore the ability of MIMO radar and coherent processing to locate a target with high resolution and to resolve targets located in the same range cell. A distributed target model is developed. It is demonstrated that MIMO radar with centralized coherent processing is able to resolve scatterers with a range resolution well beyond that supported by the signal bandwidth. The location estimation capabilities are further illustrated by introducing a new two-dimensional ambiguity function. The analysis is discussed in the context of established results for randomly thinned arrays. The investigation of high resolution MIMO radar also includes comparison with the performance of non-coherent MIMO radar and the effect on performance of the number of sensors and their locations.

I. INTRODUCTION

Inspired by the success of Multiple Input Multiple Output (MIMO) schemes in communications, we have been investigating the potential of MIMO radar systems, [1], [2]. MIMO communications has the great ability to apply diversity techniques to overcome impairments in the multipath fading channel. Accordingly, our work so far has been aimed at exploring how transmit diversity can be utilized in a MIMO radar system to overcome the target's RCS fluctuations, [2], or how combined transmit and receive diversity can be applied in target detection, [1]. Achieving spatial diversity in radar requires large inter-element distances to ensure that a target is observed from different aspects. As the different aspects are presenting uncorrelated target responses, our previous work has been based on non-coherent processing.

In this publication, we seek to explore the potential of MIMO systems to locate a single point scatterer or separate between several of those, with coherent processing applied over a sparse MIMO aperture. Our focus is on systems with multiple transmitters and receivers; a system with a single transmitter is discussed in [3].

The work of N. H. Lehmann and A. M. Haimovich was supported by the Air Force Office of Scientific Research agreement no. FA9550-06-1-0026.

The work of R. S. Blum was supported by the Air Force Research Laboratory under grant no. FA9550-06-1-0046.

In general, the range resolution of a radar system is determined by the signal bandwidth employed. We will demonstrate that coherent processing over widely dispersed sensor elements that partly surround the target may lead to resolutions higher than supported by the radar bandwidth.

The paper is organized as follows: first, a signal model for a single scatterer is developed. Based on this model, the ambiguity function for a two dimensional target location estimation is introduced. Afterwards, theoretical bounds for the location estimation accuracy of a single scatterer are introduced and compared to simulation results. The bounds are then linked to properties of the ambiguity function. This leads to a further exploration of the ambiguity function and of how system parameters, such as signal bandwidth and angular spread of the MIMO elements, determine the shape of this ambiguity function. Finally, an example of resolving several scatterers is presented.

II. SIGNAL MODEL AND AMBIGUITY FUNCTION

To illustrate the potential of high resolution approaches in MIMO-radar, this paper explores first the accuracy, with which a single scatterer can be located by a coherent array consisting of widely separated elements, similar to [3], [4]. The single point scatterer is assumed to reflect isotropically all impinging waves to all receive elements, thus allowing the coherent processing among the elements. However, the reflection coefficient of the scatterer is assumed to be unknown. For simplicity, the target is assumed located in a two dimensional (rather than three dimensional) space. The location of the scatterer is to be determined within a limited area that may be determined by a previously *non-coherent* detection mode, [5]. It is convenient to introduce a coordinate system with the origin at the center of the area and to estimate the scatterer location $\vec{X} = [x, y]^T$ relative to this origin. Figure 1 illustrates the setup. The k -th transmit and l -th receive elements, respectively, are located at angles θ_k^t and θ_l^r with respect to the origin, as illustrated in Figure 1. We assume the monitored area to be small compared to the distances from the origin to all transmitters and receivers, such that if the origin would be moved to any point in the monitored area, the angles θ_k^t and θ_l^r , would not change for all k, l . In this publication, we focus on scenarios in which the elements surround the scatterer partly, thus, e.g., $|\theta_k^t| \leq 90^\circ$ and $|\theta_l^r| \leq 90^\circ$.

Moreover, we simplify the discussion by assuming that the phases and the time references at the transmit and receive elements are calibrated to a hypothetical scatterer location at

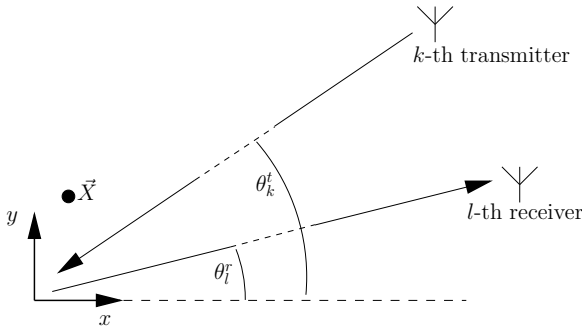


Fig. 1. Overview of system layout.

the origin of the above mentioned coordinate system. We also assume that the signal attenuation due to the distance from the transmitter or receiver to the target scatterer is approximately constant and it will be neglected in time delay calculations. Furthermore, a single snapshot (or pulse) is considered. The waveform transmitted by the k -th transmitter and reflected by a scatterer located at \vec{X} leads to a signal component at the l -th receiver of the following form

$$r_{k,l}(t) = a s_k(t - \tau_{k,l}(\vec{X})) + n_{k,l}(t), \quad (1)$$

where a contains the reflectivity of the scatterer, $n_{k,l}(t)$ is white Gaussian noise, and $\tau_{k,l}(\vec{X})$ is the delay for the k, l transmit–receive pair introduced by the scatterer location \vec{X} ,

$$\tau_{k,l}(\vec{X}) = -\frac{x}{c}(\cos \theta_k^t + \cos \theta_l^r) - \frac{y}{c}(\sin \theta_k^t + \sin \theta_l^r). \quad (2)$$

Hereafter, the explicit dependency of $\tau_{k,l}$ on \vec{X} is omitted for conciseness. The signals in (1) are of the form $r_{k,l}(t) = r_{k,l}^b(t) e^{j2\pi f_c t}$ and $s_k(t) = s_k^b(t) e^{j2\pi f_c t}$, where $r_{k,l}^b(t)$ and $s_k^b(t)$ denote the lowpass equivalent signals and f_c is the carrier frequency. Assuming that the transmitted waveforms maintain approximate orthogonality even for different mutual delays, $\int s_k^b(t) s_{k'}^{b*}(t - \tau) dt \approx 0 \quad \forall \tau, k \neq k'$, the receiver elements can separate the signals from different transmitters. The received signals over the complete system may then be represented by a $MN \times 1$ vector function $\mathbf{r}(t) = [r_{1,1}(t), \dots, r_{M,N}(t)]^T$. The noise components are assumed to be independent identical distributed (i.i.d.) Gaussian with zero mean and variance σ^2 . Therefore, the probability density function (pdf) of the received signal vector given a scatterer at \vec{X} with reflectivity a can readily be expressed as

$$\begin{aligned} & f(\mathbf{r}(t)|\vec{X}, a) \\ & \propto \exp \left\{ -\frac{1}{\sigma^2} \sum_{k=1}^M \sum_{l=1}^N \int_{-\infty}^{\infty} |r_{k,l}(t) - a s_k(t - \tau_{k,l})|^2 dt \right\} \\ & = \exp \left\{ -\frac{1}{\sigma^2} \left(\sum_{k=1}^M \sum_{l=1}^N \int_{-\infty}^{\infty} |r_{k,l}(t)|^2 + |a|^2 |s_k(t - \tau_{k,l})|^2 dt \right. \right. \\ & \quad \left. \left. - 2\Re \left\{ a \sum_{k=1}^M \sum_{l=1}^N \int_{-\infty}^{\infty} r_{k,l}^*(t) s_k(t - \tau_{k,l}) dt \right\} \right) \right\}. \end{aligned} \quad (3)$$

It is noted that in (3), the only term depending on the actual scatterer position is the third summand. Assuming unit norm waveforms, the second summand can be expressed as $\sum_{k=1}^M \sum_{l=1}^N \int |a|^2 |s_k(t - \tau_{k,l})|^2 dt = MN|a|^2$. We use the maximum likelihood estimate of the unknown scatterer reflectivity a , which is

$$\hat{a} = \frac{1}{MN} \sum_{k=1}^M \sum_{l=1}^N \int r_{k,l}(t) s_k^*(t - \tau_{k,l}) dt, \quad (4)$$

to eliminate a in (3). Then the logarithm of the pdf of the received signal (log-likelihood function of \vec{X}) is given as

$$\ln f(\mathbf{r}(t)|\vec{X}) = c' \left| \sum_{k=1}^M \sum_{l=1}^N \int r_{k,l}^*(t) s_k(t - \tau_{k,l}) dt \right|^2 + c'' \quad (5)$$

$$= c' \left| \sum_{k=1}^M \sum_{l=1}^N e^{-j2\pi f_c \tau_{k,l}} \int r_{k,l}^{b*}(t) s_k^b(t - \tau_{k,l}) dt \right|^2 + c'', \quad (6)$$

where c' and c'' denote constants independent of the scatterer location. The expression in (6) separates the phase shifts due to the carrier frequency from the baseband correlation processes. Note, these phase shifts can only be observed in a coherent processing mode across all elements. The maximum likelihood estimate of the scatterer location, $\hat{\vec{X}}$, is then given as

$$\max_{\vec{X}} \ln f(\mathbf{r}(t)|\vec{X}) = \ln f(\mathbf{r}(t)|\hat{\vec{X}}). \quad (7)$$

In a later section, the empirical variance of this estimate is found using Monte Carlo simulations, and this variance is compared to the Cramer Rao lower bound.

III. AMBIGUITY FUNCTION

An intuitive way to illustrate high resolution location estimation is to introduce the *ambiguity function* $A(\vec{X})$. The notion of an ambiguity function has long been used in the context of location estimates in radar, e.g. [6]. “Placing” a scatterer at the origin of the coordinate system, which implies $r_{k,l}(t) = s_k(t)$, the ambiguity function may be defined as a scaled version of the log-likelihood expression given in (5) and (6),

$$\begin{aligned} A(\vec{X}) &= d' \ln f(\mathbf{r}(t)|\vec{X}) + d'' \quad (8) \\ &= \frac{1}{M^2 N^2} \left| \sum_{k=1}^M \sum_{l=1}^N \int s_k^*(t) s_k(t - \tau_{k,l}) dt \right|^2 \\ &= \frac{1}{M^2 N^2} \left| \sum_{k=1}^M \sum_{l=1}^N e^{-j2\pi f_c \tau_{k,l}} \int s_k^{b*}(t) s_k^b(t - \tau_{k,l}) dt \right|^2. \end{aligned}$$

The constants d' and d'' scale the ambiguity in such manner that $0 \leq A(\vec{X}) \leq 1$ is ensured.

Figure 2 contains a plot of an ambiguity function of an example of a 9×9 MIMO system with the transmitter elements distributed evenly over $-45^\circ \leq \theta \leq 45^\circ$. The

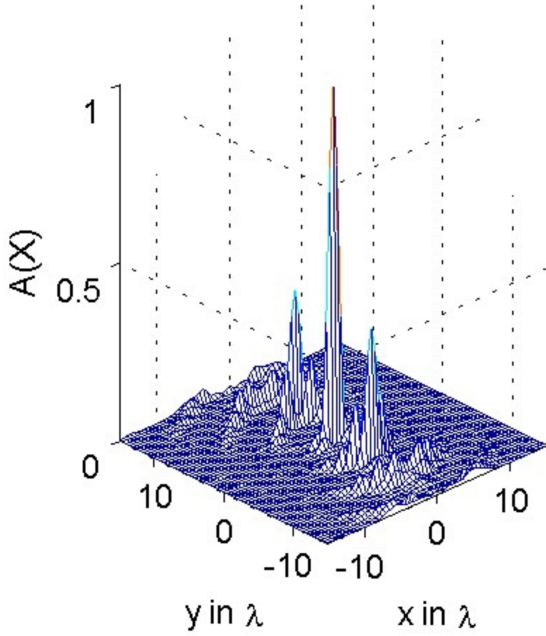


Fig. 2. Ambiguity Function for a 9×9 MIMO-radar.

receiver elements are similarly distributed. A x and y cut of this ambiguity function can be found in Figures 3 and 4, respectively, together with the cuts of the non-coherent ambiguity function introduced in the sequel.

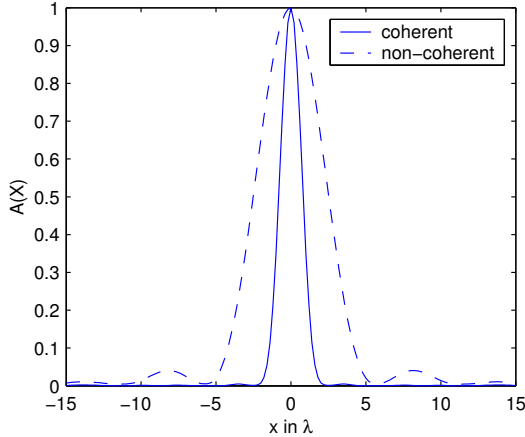


Fig. 3. x cut of the coherent and non-coherent Ambiguity Function.

The transmitted signals $s_k(t)$ are assumed to have an ideal rectangular frequency response with bandwidth Δf . The ratio of this bandwidth to the carrier frequency is set to one tenth, $\frac{\Delta f}{f_c} = 0.1$. The choice of this value is briefly discussed in the sequel. The x and y coordinates are expressed in multiples of the carrier wavelength λ . The narrow mainlobe around the origin demonstrates the potential of coherent processing in MIMO radar.

The integrals in the sums of the last line of (8) are the autocorrelation functions of the waveforms $\int s_k^{b*}(t)s_k^b(t-\tau) =$

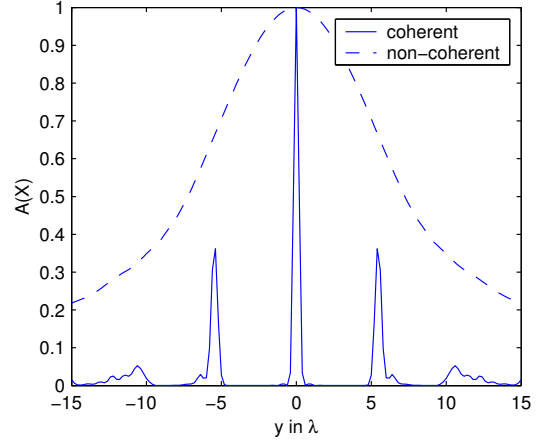


Fig. 4. y cut of the coherent and non-coherent Ambiguity Function.

$\varphi_{s_k^b}(\tau)$. Accordingly, the ambiguity function can be rewritten as

$$A(\vec{X}) = \frac{1}{M^2 N^2} \left| \sum_{k=1}^M \sum_{l=1}^N e^{-j2\pi f_c \tau_{k,l}} \varphi_{s_k^b}(\tau_{k,l}) \right|^2, \quad (9)$$

which further illustrates the role of the phase shifts across the transmitter–receiver pairs in the coherent processing. The impact of these phase shifts is further illuminated by introducing the *non-coherent* ambiguity function, $A_{nc}(\vec{X})$, which serves as an upper bound for the coherent ambiguity function,

$$A(\vec{X}) \leq A_{nc}(\vec{X}) = \frac{1}{M^2 N^2} \left(\sum_{k=1}^M \sum_{l=1}^N |\varphi_{s_k^b}(\tau_{k,l})| \right)^2. \quad (10)$$

Note that the non-coherent ambiguity function serves as an upper bound to the coherent ambiguity function. This function illustrates the location accuracy possible for a MIMO system with non-coherent processing among the elements. The location estimate is then strongly dependent on the bandwidth of the transmitted waveforms. The non-coherent ambiguity function is plotted in Figure 5 for the same example system as before.

By comparing the two plots in Figures 2 and 5 or the cuts in Figures 3 and 4, it becomes evident how coherent processing enhances the resolution by substantially narrowing the mainlobe of the ambiguity function. Moreover, Figures 3 and 4 illustrate how the non-coherent ambiguity function serves as an upper bound of the coherent ambiguity function.

This section is concluded by demonstrating the ability of a MIMO-radar system to resolve several closely spaced scatterers. Figure 6 features the ambiguity function for four equal return point scatterers at locations $[0, 0]^T$, $[0, 6]^T$, $[6, 0]^T$ and $[6, 6]^T$. The coordinate system is again expressed in multiples of λ .

Comparing this plot to the non-coherent case in Figure 5, it is obvious, that a coherent MIMO radar can resolve several closely spaced scatterers. These scatterers might either constitute a single target with multiple, resolvable scatterers or represent separate, small targets.

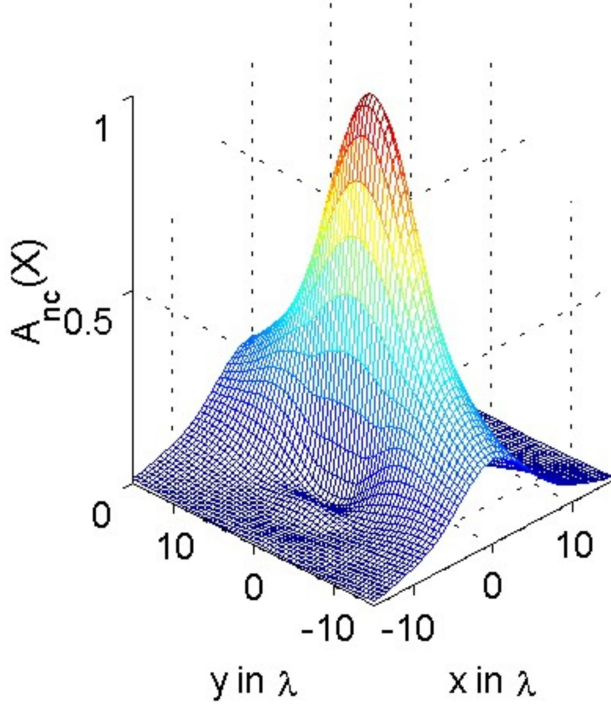


Fig. 5. Non-coherent Ambiguity Function for a 9×9 MIMO-radar.

IV. CRAMER RAO BOUND

As discussed in [7], the Cramer Rao Bound (CRB) for a parameter vector, ψ , to be estimated is given as

$$E \left\{ (\hat{\psi} - \psi)(\hat{\psi} - \psi)^H \right\} \geq \mathbf{C}_{CRB}(\psi) = \mathbf{J}^{-1}(\psi), \quad (11)$$

where the inequality implies that the difference between the first and the second matrix is a positive definite matrix¹. The CRB provides a lower bound for the mean square error (MSE) of any unbiased estimator for the unknown parameters ψ_i . This is expressed by [8]

$$\text{var}\{\hat{\psi}_i\} \geq [\mathbf{J}^{-1}(\psi)]_{i,i}. \quad (12)$$

In the scenario discussed here, the parameter vector ψ contains the x and y coordinates of the scatterer and the real and imaginary part of the common amplitude of the reflected signal, a_r and a_i , i.e. $\psi = [x, y, a_r, a_i]^T$. In both equations, $\mathbf{J}(\psi)$ refers to the Fisher information matrix, which is defined as

$$\begin{aligned} \mathbf{J}(\psi) &= E \left\{ \nabla_{\psi} \ln f(\mathbf{r}(t)) (\nabla_{\psi} \ln f(\mathbf{r}(t)))^H \right\} \\ &= -E \left\{ \nabla_{\psi} (\nabla_{\psi} \ln f(\mathbf{r}(t)))^H \right\}. \end{aligned} \quad (13)$$

Introducing an alternative parameter vector, ϑ , the chain rule can be used with the first equality of (13), [9],

$$\begin{aligned} \mathbf{J}(\psi) &= \nabla_{\psi} \vartheta^H E \left\{ \nabla_{\vartheta} \ln f(\mathbf{r}) (\nabla_{\vartheta} \ln f(\mathbf{r}))^H \right\} (\nabla_{\psi} \vartheta^H)^H \\ &= \mathcal{G} \mathbf{J}(\vartheta) \mathcal{G}^H. \end{aligned} \quad (14)$$

¹The superscript H denotes the conjugate transposed.

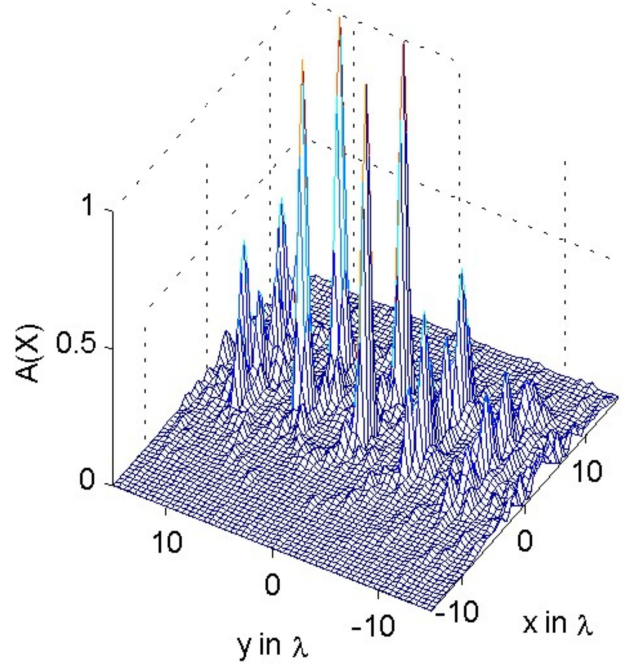


Fig. 6. Ambiguity Function for four scatterers in close proximity and a 9×9 MIMO-radar.

Consider a particular ϑ , that contains the $M \cdot N$ time delays $\tau_{k,l}$ and the complex amplitude pair a_r and a_i such that

$$\vartheta = [\tau_{1,1}, \dots, \tau_{k,l}, \dots, \tau_{M,N}, a_r, a_i]^T. \quad (15)$$

The $4 \times (M \cdot N + 2)$ matrix \mathcal{G} mainly describes the geometric setting and has, according to the signal model (2), the form

$$\mathcal{G} = \begin{pmatrix} -\frac{1}{c} (\cos \theta_1^t + \cos \theta_1^r) & \dots & -\frac{1}{c} (\cos \theta_M^t + \cos \theta_M^r) & 0 & 0 \\ -\frac{1}{c} (\sin \theta_1^t + \sin \theta_1^r) & \dots & -\frac{1}{c} (\sin \theta_M^t + \sin \theta_M^r) & 0 & 0 \\ 0 & \dots & 0 & 1 & 0 \\ 0 & \dots & 0 & 0 & 1 \end{pmatrix}. \quad (16)$$

Given the density of the received signal (3), $\mathbf{J}(\vartheta)$ is subsequently evaluated. First,

$$\begin{aligned} \frac{\delta \ln f(\mathbf{r})}{\delta \tau_{k,l}} &= \frac{-1}{\sigma^2} \int (r_{k,l}(t) - a s_k(t - \tau_{k,l})) a^* \dot{s}_k^*(t - \tau_{k,l}) \\ &\quad + (r_{k,l}(t) - a s_k(t - \tau_{k,l}))^* a \dot{s}_k(t - \tau_{k,l}) dt, \end{aligned} \quad (17)$$

with $\dot{s}_k(t) = \frac{\delta}{\delta t} s_k(t)$. This readily leads to

$$E \left\{ \frac{\delta^2 \ln f(\mathbf{r})}{\delta \tau_{k,l} \delta \tau_{k',l'}} \right\} = 0 \quad \forall l \neq l' \text{ or } k \neq k'. \quad (18)$$

One finds for the $M \cdot N$ diagonal elements of $\mathbf{J}(\vartheta)$

$$E \left\{ \frac{\delta^2 \ln f(\mathbf{r})}{\delta \tau_{k,l}^2} \right\} = \frac{-2|a|^2}{\sigma^2} \int \dot{s}_k(t - \tau_{k,l}) \dot{s}_k^*(t - \tau_{k,l}) dt, \quad (19)$$

$$\mathbf{J}(\boldsymbol{\psi}) = \begin{pmatrix} \frac{8\pi^2|a|^2}{\lambda^2 N_0} \left(1 + \frac{\beta^2}{f_c^2}\right) \sum_{k=1}^M \sum_{l=1}^N \mathcal{X}_{k,l}^2 & \frac{8\pi^2|a|^2}{\lambda^2 N_0} \left(1 + \frac{\beta^2}{f_c^2}\right) \sum_{k=1}^M \sum_{l=1}^N \mathcal{X}_{k,l} \mathcal{Y}_{k,l} & \frac{-4\pi a_i}{\lambda N_0} \sum_{k=1}^M \sum_{l=1}^N \mathcal{X}_{k,l} & \frac{4\pi a_r}{\lambda N_0} \sum_{k=1}^M \sum_{l=1}^N \mathcal{X}_{k,l} \\ \frac{8\pi^2|a|^2}{\lambda^2 N_0} \left(1 + \frac{\beta^2}{f_c^2}\right) \sum_{k=1}^M \sum_{l=1}^N \mathcal{X}_{k,l} \mathcal{Y}_{k,l} & \frac{8\pi^2|a|^2}{\lambda^2 N_0} \left(1 + \frac{\beta^2}{f_c^2}\right) \sum_{k=1}^M \sum_{l=1}^N \mathcal{Y}_{k,l}^2 & \frac{-4\pi a_i}{N_0} \sum_{k=1}^M \sum_{l=1}^N \mathcal{Y}_{k,l} & \frac{4\pi a_r}{N_0} \sum_{k=1}^M \sum_{l=1}^N \mathcal{Y}_{k,l} \\ \frac{-4\pi a_i}{\lambda N_0} \sum_{k=1}^M \sum_{l=1}^N \mathcal{X}_{k,l} & \frac{-4\pi a_i}{\lambda N_0} \sum_{k=1}^M \sum_{l=1}^N \mathcal{Y}_{k,l} & \frac{2MN}{N_0} & 0 \\ \frac{4\pi a_r}{\lambda N_0} \sum_{k=1}^M \sum_{l=1}^N \mathcal{X}_{k,l} & \frac{4\pi a_r}{\lambda N_0} \sum_{k=1}^M \sum_{l=1}^N \mathcal{Y}_{k,l} & 0 & \frac{2MN}{N_0} \end{pmatrix} \quad (32)$$

where $E \left\{ \int (r_{k,l}(t) - a s_k(t - \tau_{k,l})) \dot{s}_k^*(t - \tau_{k,l}) dt \right\} = 0$ is used (the white noise is uncorrelated to the transmitted waveforms and their derivatives). This equality furthermore is used to derive the following two relations:

$$E \left\{ \frac{\delta^2 \ln f(\mathbf{r})}{\delta \tau_{k,l} \delta a_r} \right\} = \frac{2}{\sigma^2} \Re \left\{ a \int \dot{s}_k(t - \tau_{k,l}) s_k^*(t - \tau_{k,l}) dt \right\}, \quad (20)$$

$$E \left\{ \frac{\delta^2 \ln f(\mathbf{r})}{\delta \tau_{k,l} \delta a_i} \right\} = \frac{2}{\sigma^2} \Im \left\{ a \int \dot{s}_k(t - \tau_{k,l}) s_k^*(t - \tau_{k,l}) dt \right\}. \quad (21)$$

It is easy to verify the following three equalities:

$$E \left\{ \frac{\delta^2 \ln f(\mathbf{r})}{\delta a_r^2} \right\} = \frac{-2}{\sigma^2} \sum_{k=1}^M \sum_{l=1}^N \int |s_k(t - \tau_{k,l})|^2 dt, \quad (22)$$

$$E \left\{ \frac{\delta^2 \ln f(\mathbf{r})}{\delta a_i^2} \right\} = \frac{-2}{\sigma^2} \sum_{k=1}^M \sum_{l=1}^N \int |s_k(t - \tau_{k,l})|^2 dt, \quad (23)$$

$$E \left\{ \frac{\delta^2 \ln f(\mathbf{r})}{\delta a_i \delta a_r} \right\} = 0. \quad (24)$$

The integrals in expressions (19) to (23) are evaluated by replacing $s_k(t)$ with $s_k^b(t) \cdot e^{j2\pi f_c t}$. For (19) this leads to

$$\int \dot{s}_k(t - \tau_{k,l}) \dot{s}_k^*(t - \tau_{k,l}) dt = 4\pi^2 \left(f_c^2 \int |S_k^b(f)|^2 df + \int f^2 |S_k^b(f)|^2 df \right) \quad (25)$$

and for (20) and (21) to

$$\int \dot{s}_k(t - \tau_{k,l}) s_k^*(t - \tau_{k,l}) dt = j2\pi f_c \int |S_k^b(f)|^2 df, \quad (26)$$

where $S_k^b(f)$ denotes the Fourier transform of $s_k^b(t)$. Using $\sigma^2 = N_0 \int |S_k^b(f)|^2 df$ and the effective bandwidth β , defined as

$$\beta^2 = \frac{\int f^2 |S_k^b(f)|^2 df}{\int |S_k^b(f)|^2 df}, \quad (27)$$

the first MN diagonal elements of $\mathbf{J}(\boldsymbol{\vartheta})$ are given as (compare to (19))

$$[\mathbf{J}(\boldsymbol{\vartheta})]_{i,i} = \frac{8\pi^2|a|^2}{N_0} (f_c^2 + \beta^2) \quad i = 1, \dots, MN. \quad (28)$$

Note, that the off-diagonal elements of the upper left $MN \times MN$ submatrix of $\mathbf{J}(\boldsymbol{\vartheta})$ are zero according to (18). The elements of the lower left $2 \times MN$ submatrix of $\mathbf{J}(\boldsymbol{\vartheta})$ are found via (20) and (21), respectively, as

$$[\mathbf{J}(\boldsymbol{\vartheta})]_{MN+1,i} = \frac{4\pi f_c a_i}{N_0} \quad i = 1, \dots, MN, \quad (29)$$

$$[\mathbf{J}(\boldsymbol{\vartheta})]_{MN+2,i} = -\frac{4\pi f_c a_r}{N_0} \quad i = 1, \dots, MN. \quad (30)$$

Furthermore, the diagonal elements of the 2×2 lower right submatrix of $\mathbf{J}(\boldsymbol{\vartheta})$ are found according to (22) and (23) as

$$[\mathbf{J}(\boldsymbol{\vartheta})]_{i,i} = \frac{2MN}{N_0} \quad i = MN + 1, MN + 2. \quad (31)$$

According to (14), $\mathbf{J}(\boldsymbol{\psi})$ can now be calculated and is provided in (32), where for conciseness $\mathcal{X}_{k,l} = \cos \theta_k^t + \cos \theta_l^r$ and $\mathcal{Y}_{k,l} = \sin \theta_k^t + \sin \theta_l^r$ is used. Note, that those terms reflect the impact of the geometric setting (the location of transmitters and receivers relative to the target) on the resolution and are due to the matrix \mathcal{G} given in (16). The lower bounds for the variance of the x and y estimates are the (1,1) and (2,2) elements of $\mathbf{J}(\boldsymbol{\psi})^{-1}$. It is noted, that these elements do not depend on the real or imaginary part of the signal amplitude, a_r or a_i , specifically, but on the signal energy $|a|^2 = a_r^2 + a_i^2$. The bounds derived above manner enable us to predict the performance of a location estimate for a single scatterer. Therefore, they can be used to judge the high resolution potential of coherent MIMO radar systems as described in the previous section and [5]. They also allow us to derive accuracy limits of approaches similar to the ones presented in [3], [4]. Furthermore, important conclusions about the effects of system parameters on the accuracy of the parameter estimation can be derived from $\mathbf{J}(\boldsymbol{\psi})$. Assuming a rectangular frequency response, $S_k^b(f)$, $f \in [-\frac{\Delta f}{2}, \frac{\Delta f}{2}]$, the

square of the effective bandwidth is found as $\beta^2 = \frac{\Delta f^2}{12}$. Therefore, even for relatively high bandwidth to carrier ratios, e.g. $\frac{\Delta f}{f_c} = 0.1$, the contribution of the signal bandwidth to the CRB is negligible as $\frac{\beta^2}{f_c^2} \ll 1$ and thus $(1 + \frac{\beta^2}{f_c^2}) \approx 1$ in the upper left submatrix of (32). However, it is noted, that by replacing $(1 + \frac{\beta^2}{f_c^2})$ with $\frac{\beta^2}{f_c^2}$ the upper left matrix in (32) becomes the Fisher information matrix, one would obtain in a non-coherent, pure time of arrival (TOA) scheme, as described in [9]. Furthermore, it is possible to conclude from (32) that the CRB's for the x and y estimates are proportional² to λ^2 and the inverse of SNR. The proportionality to λ^2 and equivalently to $\frac{1}{f_c^2}$ is due to the fact that the coherent MIMO-system makes use of the phase information across different paths, as, for example, equation (6) illustrates.

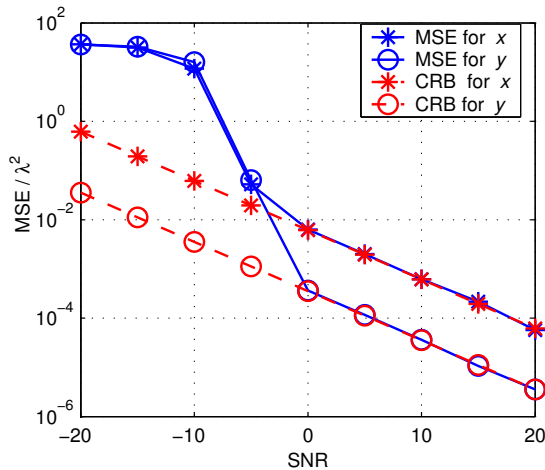


Fig. 7. MSE of ML estimate and CRB for a 9×9 high resolution MIMO radar.

In Figure 7, the bounds and the MSE of the x and y estimates based upon the maximum likelihood estimation described in (7) are plotted. Note, that the ordinate is given in multiples of λ^2 . The underlying scenario is the 9×9 system introduced in the previous section. The MSE is obtained from Monte Carlo simulations with 2000 iterations per SNR value. The empirical MSE and the theoretical bounds are in excellent agreement for high SNR values. For low SNR, the classical *threshold* effect, well known in time of arrival and angle estimates, is observed. Further, it is observed that the precision of the x and y estimates differ. This is due to the geometry of the considered sensor locations. The ambiguity functions in Figures 2, 3 and 4 are based on the same system layout. Particularly, the x and y cuts in Figures 3 and 4 show a much more narrow coherent mainlobe in y than in x direction. Accordingly, the estimation precision in the y direction has to be higher than in the x direction.

²Assuming a constant $\frac{\Delta f}{f_c}$.

Even though the employed bandwidth has a very limited impact on the high SNR system performance (as discussed above), it has to be noted that it plays a crucial role in limiting the amount of the with the mainlobe competing sidelobes. Indeed it can be extrapolated from the work of Steinberg et al., [10], [11], that for random receive and transmit element locations the peak sidelobe ratio (PSLR) is proportional to $\ln(\frac{f_c}{\Delta f})$. Furthermore, the PSLR is proportional to $\frac{1}{MN}$ which motivates the use of multiples of both, receive *and* transmit antennas. However, further work has to be undertaken to gain better insights into the importance of these system parameters.

V. CONCLUSIONS

In this paper, we discussed the high resolution capabilities of a coherent MIMO radar system with widely separated array elements on the transmit and receive sides. By comparing the coherent and non-coherent ambiguity function, we illustrated that the phase shifts across the different antenna elements and therefore the system wide coherent processing provide the basis for high accuracy. We established the non-coherent ambiguity function as an upper bound of the coherent one. Furthermore, we illustrated with one example that coherent MIMO processing is capable to resolve scatterers or targets separated by less than the signal bandwidth. Moreover, we presented Cramer Rao bounds enabling to predict the location estimation performances of coherent MIMO radar systems. Finally we linked the with those bounds predicted accuracy to the shape of the coherent ambiguity function.

REFERENCES

- [1] E. Fishler, A. H. Haimovich, R. S. Blum, L. Cimini, D. Chizhik, and R. Valenzuela, "Spatial diversity in radars - models and detection performance," *IEEE Trans. on Signal Processing*, vol. 54, no. 3, pp. 823–838, March 2006.
- [2] N. Lehman, E. Fishler, A. M. Haimovich, R. S. Blum, L. Cimini, and R. Valenzuela, "Evaluation of Transmit Diversity in MIMO-radar Direction Finding," *accepted by IEEE Trans. on Signal Processing*, 2006.
- [3] D. R. Kirk, J. S. Bergin, P. M. Techau, and J. E. Don Carlos, "Multi-Static Coherent Sparse Aperture Approach to Precision Target Detection and Engagement," *IEEE International Radar Conference*, pp. 579–584, May 2005.
- [4] J. E. Don Carlos, D. R. Kirk, J. S. Bergin, P. M. Techau, and J. D. Halsey, "Detecting system having a coherent sparse aperture," U.S. Patent 6,724,340, April 20, 2004.
- [5] R. S. Blum, L. Cimini, and A. H. Haimovich, "MIMO-Radar: Part 1 – Concepts and Applications," *IEEE Signal Processing Magazine (in preparation)*, 2006.
- [6] N. Levanon, *Radar Principles*. John Wiley & Sons, 1988.
- [7] H. L. V. Trees, *Optimum Array Processing*, 1st ed. John Wiley, 2003.
- [8] S. M. Kay, *Fundamentals of Statistical Signal Processing: Estimation Theory*, 1st ed. Prentice Hall PTR, 1993, vol. 1.
- [9] Y. Qi, H. Kobayashi, and H. Suda, "Analysis of Wireless geolocation in a Non-Line-of-Sight Environment," *IEEE Trans. on Wireless Communications*, vol. 5, no. 3, pp. 672–681, March 2006.
- [10] B. D. Steinberg and E. H. Attia, "Sidelobe Reduction of Random Arrays by Element Position and Frequency Diversity," *IEEE Transactions on Antennas and Propagation*, vol. AP-31, no. 6, pp. 922–930, November 1983.
- [11] B. D. Steinberg, "The Peak Sidelobe of the Phased Array Having Randomly Located Elements," *IEEE Transactions on Antennas and Propagation*, vol. AP-20, no. 2, pp. 129–136, March 1972.